Locations and types of ruptures involved in the 2008 Sichuan earthquake inferred from SAR image matching

Tomokazu Kobayashi,[1] Youichiro Takada,[2] Masato Furuya,[2] and Makoto Murakami[1]

Received 4 December 2008; revised 21 February 2009; accepted 26 February 2009; published 1 April 2009.

[1] We have detected detailed ground displacements in the proximity of the Longmen Shan fault zone (LMSFZ) by applying a SAR offset-tracking method in the analysis of the 2008 Sichuan earthquake. An elevation-dependent correction is indispensable for achieving sub-meter accuracy. A sharp displacement discontinuity with a relative motion of ~1–2 m appears over a length of 200 km along the LMSFZ, which demonstrates that the main rupture has proceeded on the Beichuan fault (BF) among several active faults composing the LMSFZ, and a new active fault is detected on the northeastward extension of the BF. The rupture on the BF is characterized by a right-lateral motion in the northeast, while in the southwest an oblique right-lateral thrust slip is suggested. In contrast to the northeast, where a major rupture proceeded on the BF only, in the southwest multiple thrust ruptures have occurred in the southeastern foot of the Pengguan massif. **Citation:** Kobayashi, T., Y. Takada, M. Furuya, and M. Murakami (2009), Locations and types of ruptures involved in the 2008 Sichuan earthquake inferred from SAR image matching, *Geophys. Res. Lett.*, *36*, L07302, doi:10.1029/2008GL036907.

1. Introduction

[2] A catastrophic earthquake with a moment magnitude of 7.9 struck China's Sichuan area on 12 May 2008 [*National Earthquake Information Center*, 2008]. This earthquake could be associated with the reactivation of the Longmen Shan fault zone (LMSFZ), running over a length of 200 km along the western margin of the Sichuan Basin (Figure 1). The fault zone consists of several faults dipping to the northwest that have been constructed in the area subjected to contractional stress due to the eastward movement of the Tibetan plateau [*Burchfiel et al.*, 2008]. The faults have a complicated development in and around the Pengguan massif (PM) (Figure 1). Three major active faults, indicated by red lines in Figure 1 [*Densmore et al.*, 2007], are running near the epicenter (red star) located at the southwestern edge of the PM. The rupture is thought to proceed northeastward along the fault zone as inferred from the extent of the aftershocks reported by the U. S. Geological Survey (black dots in Figure 1), but it remains uncertain where and how the faults were involved in the seismic event [*Burchfiel et al.*, 2008]. The measurement of ground displacements around the epicentral area certainly plays a key role in answering these questions.

[3] Satellite synthetic aperture radar (SAR) data can provide detailed and spatially comprehensive ground information. Interferometric SAR (InSAR) analysis has an advantage of detecting ground deformation in a vast region with high precision [e.g., *Massonnet and Feigl*, 1998; *Bürgmann et al.*, 2000]. However, for the Sichuan event, the standard InSAR approach is not helpful in knowing the faults directly related to the seismic rupture. This is because the displacement amplitude near the fault zone was too large and a coherent loss area which spreads over an area ~200 km long and ~10–30 km wide prevents us from satisfactorily obtaining the ground deformation in the proximity of the fault zone. Thus, in order to reveal the unknown surface displacements, we conduct an offset-tracking procedure that enables us to robustly detect large ground deformation even in an incoherent area [*Michel et al.*, 1999; *Tobita et al.*, 2001; *Pathier et al.*, 2006]. While similar approaches can be taken with optical images [e.g., *Avouac et al.*, 2006], SAR images are advantageous because of the radar's all-weather detection capability.

2. SAR Data Analysis

[4] We use ALOS/PALSAR data on the ascending orbital paths 471 to 476 (Table S1) for data analysis.[1] The data obtained is strip-map imagery with an incidence angle of 38.7°. The analyzed areas are indicated by blue frames in the inset of Figure 1. We process the SAR data from a level-1.0 product using a software package Gamma [*Wegmüller and Werner*, 1997]. After conducting coregistration between two images acquired before and after the mainshock, we divide the single-look SAR amplitude images into patches and calculate an offset between the corresponding patches by an intensity tracking method. This method is performed by cross-correlating samples of backscatter intensity of a master image with those of a slave image [*Strozzi et al.*, 2002]. We now employ a near-square search patch of 64 × 192 pixels (range × azimuth, ~480 m × 610 m on the ground) and a sampling interval of 36 × 108 pixels (~270 m × 340 m on the ground). The measured offset consists of two components: (1) displacement along the line of sight (range offset) and (2) a horizontal movement on the ground, parallel along the satellite track (azimuth offset).

[5] Accuracy of offset measurement depends strongly on the quality of image coregistration, and thus, we carry out an additional operation that is not necessary over a flat area: a correction of stereoscopic effect [*Michel et al.*, 1999;

[1]Institute of Seismology and Volcanology, Graduate School of Science, Hokkaido University, Sapporo, Japan.
[2]Department of Natural History Sciences, Graduate School of Science, Hokkaido University, Sapporo, Japan.

0094-8276/09/2008GL036907

[1]Auxiliary materials are available in the HTML. doi:10.1029/2008GL036907.

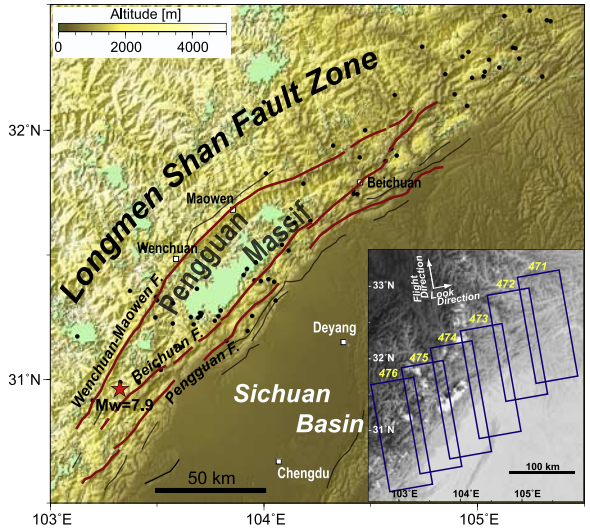

Figure 1. Tectonic setting of the Longmen Shan fault zone. Topographic relief map is taken from the SRTM DEM data with a resolution of 3 arcsecs. Light green colored areas in the relief indicate lacks of DEM data. The epicenter is marked with a star, and the aftershocks that occurred from 12–19 May are shown as black dots [*National Earthquake Information Center*, 2008]. Solid lines are fault traces drawn after *Densmore et al.* [2007], and the red lines stand for the Wenchuan-Maowen, Beichuan, and Pengguan faults, which are active faults that compose the majority of the Longmen Shan fault zone. Analyzed regions are indicated by blue frames in the inset.

Pathier et al., 2006]. Besides the actual surface displacements, range offsets include artifact offsets over rugged terrain, resulting from a difference in foreshortening effect caused by separation between the satellite orbital tracks. Thus, we reduce the artifact by applying an elevation-dependent correction incorporating SRTM (NASA's Shuttle Radar Topography Mission) DEM data with a 3 arcsec resolution [*Farr et al.*, 2007].

3. Ground Displacements for the 2008 Sichuan Earthquake

[6] Figure 2 shows the estimated range offset field over the entire analyzed area. The offset analysis succeeded in mapping the ground displacement in the proximity of the fault zone, which was difficult to achieve from the standard InSAR approach. The most notable feature is a sharp color discontinuity over a length of about 200 km, across which the ground movement is in the opposite direction (solid line). The boundary extends continuously in the northeast-southwest orientation, running just along the LMSFZ. The movement in the northern side of the boundary is away from the satellite (red), while that in the southern side is towards the satellite (blue). A major displacement field is localized within a zone no wider than several tens of kilometers, and the amount of relative displacement near the boundary reaches up to ~2 m. It should now be noted that the displacement boundary is in very good agreement with the Beichuan fault (BF) trace (dotted line), suggesting that a main rupture proceeded on the BF. This is the first published information from satellite data that mentions the fault as a major contributor to the earthquake rupture. Further a noteworthy accomplishment is that we detected a new active fault. A displacement boundary clearly appears not only on the BF trace (dotted line) which has been identified as an active fault [*Densmore et al.*, 2007] but also on its northeastward extension (Figure 2). We stress that the location of the active fault, namely the BF, is confirmed not from the geomorphological observations but from the actual surface displacements associated with the earthquake.

[7] The original azimuth offset field (Figure S1a) suffers from periodic offset patterns that are presumably ionosphere-related noises [*Gray et al.*, 2000; *Wegmüller et al.*, 2006]. In order to reduce the oscillatory noises, we apply a band-cut filter through which the wavenumbers corresponding to the noises are removed. The detailed method is shown in the auxiliary material (Figure S2). After filtering, in the azimuth offset field (Figure S1b), displacement boundaries turn out to be in the proximity of the fault zone (solid lines). However, the spatial pattern is slightly different from the range offset. In the northeast of the fault zone, the displacement boundary overlaps the BF (dotted line) and its extension in the same location as the range offset result, but in the southwest the boundary on the BF is not clear and a new discontinuity is identified at a different location. The rupture style of this seismic event seems to be more complex than that expected from the range offset field. In the following, we focus on the paths 472 and 474, in which the azimuth noises are suppressed well by filtering, and investigate more detailed features of the ruptures in the northeast and in the southwest.

[8] The rupture type on the BF is different between in the northeast and in the southwest. Figure 3a shows the offset field in the northeast of the BF (path 472) in range (Figure 3a, left) and azimuth (Figure 3a, right). The range offset shows that the movement in the northern side of the displacement boundary (solid line) is away from the satellite (red) and that in the southern side is toward the satellite (blue), while for the azimuth offset the movements in the northern and southern sides are toward (red) and opposite to (blue) the satellite flight direction, respectively. Taking four simple fault types into account; reverse, normal, right-lateral, and left-lateral motions, the fault motion that can account for the observed displacement pattern is a right-lateral slip. The displacement vector field, obtained from an assumption that the observed offsets are produced by only horizontal movements on the ground, shows a nearly pure right-lateral fault motion of approximately 2 m (Figure S3).

[9] On the other hand, in the southwest on the BF (path 474) the fault motion is slightly more complex (Figure 3b). A displacement boundary on the BF that is observed from both the offset fields in the northeast (Figure 3a) is not distinct in the azimuth field (Figure 3b, right), although the boundary is clearly visible in the range (solid line in Figure 3b, left). This suggests that the observed displacement can be explained by neither a pure dextral strike-slip nor a pure reverse fault motion. The preferred rupture style is a composite motion including both right-lateral and reverse slip components.

[10] The outline of the inferred fault motions is illustrated in Figure 4. The obtained offset field reveals that the main rupture occurred on the BF and its rupture style is charac-

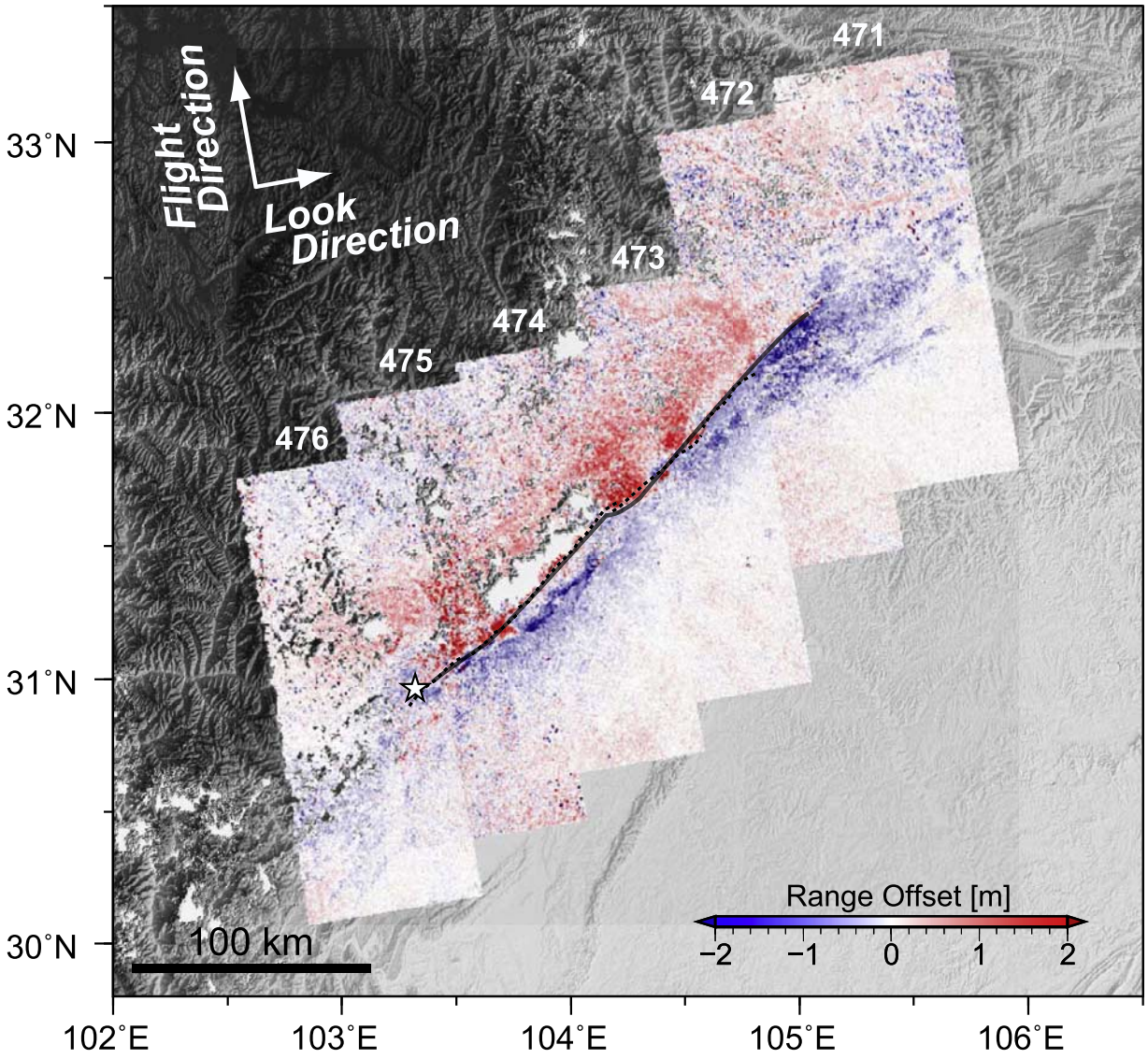

Figure 2. Displacement field in range component. Warm and cold colors represent displacements away from and toward the satellite, respectively. A sharp color discontinuity, across which the ground motion is in the opposite direction, is highlighted with a solid line, and is recognized to be just along the Beichuan fault trace indicated by a dotted line.

terized by a right-lateral motion in the northeast and an oblique right-lateral thrust slip in the southwest. The result inferred from the offset analysis has a good agreement with that of the preliminary teleseismic waveform analysis showing that the Sichuan event slipped right-laterally in the northeast and in the southwest with a right-lateral thrust component [e.g., *Nishimura and Yagi*, 2008]. The difference in the northeast and southwest fault-motion types may suggest that the BF is segmented at the north end of the PM, which corresponds to a geological boundary [*Burchfiel et al.*, 2008].

[11] In contrast to the northeastern part of the LMSFZ where the observations can be accounted for a relatively simple motion on the BF, the offset fields in the southwest are suggestive of complicated ground deformations. In the southeastern flank of the PM (inset of Figure 3b), a clear displacement boundary with a relative motion of nearly 1 m can be observed over a length of ~50 km in the azimuth offset field (arrows in Figure 3b, right). A large offset of ~2 m moving toward the satellite, featured with arrows (inset in Figure 3b, left), appears around the corresponding area in the range offset field. The deforming area is obviously distant from the BF (dotted line in the inset), thus indicating occurrence of another regional rupture. The detected rupture is traced near the Pengguan fault (PF) as mapped by *Densmore et al.* [2007] but does not completely correspond to the PF trace in the azimuth offset (dotted line in Figure 3b). Thus we do not argue at present to what extent the deformation is related to the PF.

[12] The displacement pattern of the regional deformation is evidently different from that observed along the BF. In the azimuth field, the movement in the northern side of the boundary is opposite to the satellite flight direction (blue), while that in the southern side is toward the flight direction (red). Thus a convergent motion is suggested because a left-lateral motion is unlikely. There is no clear displacement discontinuity in the range, indicating no significant strike-slip motion but probably an upheaval. Thus we can say that

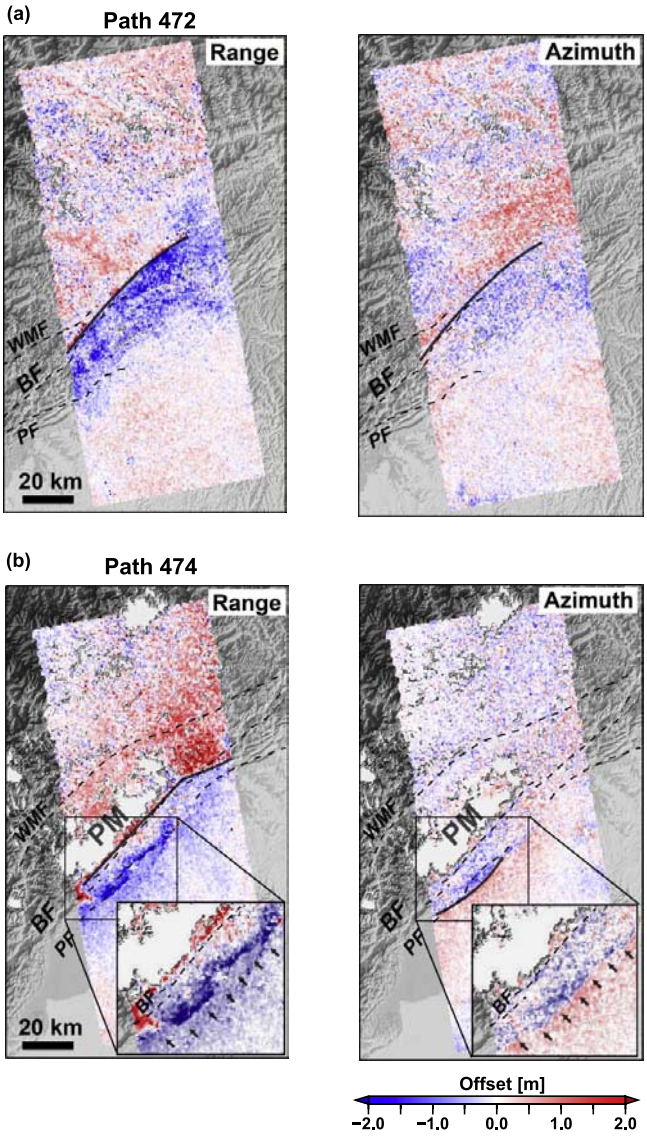

Figure 3. Displacement field for the paths (a) 472 and (b) 474 in (left) range and (right) azimuth components, respectively. In the range offset field, warm and cold colors stand for displacements away from and toward the satellite, respectively, and in the azimuth toward and opposite the satellite flight direction, respectively. Displacement boundaries are highlighted with solid lines. Arrows in the inset of the range and azimuth fields features a deforming area located at the southeastern foot of the Pengguan massif. WMF, Wenchuan-Maowen fault; BF, Beichuan fault; PF, Pengguan fault; and PM, Pengguan massif.

the local deformation is of a reversed fault type. The offset result shows that in the southwest of the LMSFZ, multiple ruptures which are different fault motions but significantly include reverse slip components occurred (Figure 4).

[13] On the other hand, there is no signal showing any significant ground deformations along the Wenchuan-Maowen fault (WMF), which is one of the major active faults composing the LMSFZ. The idea that no significant rupture occurred on the WMF is in harmony with the observation that the aftershocks mainly distribute around the BF rather than the WMF (Figure 1).

[14] With the knowledge of the locations of main ruptures, we constructed a preliminary fault model that consists of three rectangular faults with distributed slips, using an elastic half-space dislocation model [*Okada*, 1992] (Table S2). The synthetic range offset field obtained from our preliminary fault model reproduces roughly the observed spatial pattern on the offset field (Figure S4). In our model, a right-lateral motion is dominant in the northeast of the BF (Figure S5a; F1), while in the southwest an oblique slip consisting of right-lateral and reverse motions is assumed (Figure S5b; F2). The rupture locally occurring near the PF is explained by a nearly pure thrust motion (Figure S5c; F3). However, there still remain significant discrepancies between the observed and calculated offset fields. A joint analysis with InSAR-based far-field displacements data will allow us to infer more quantitative and detailed fault model, and is deferred for future studies.

4. Uncertainties and Reliabilities of Measured Offsets

[15] To confirm how much errors are included in the measured offset fields, we calculate offsets using two preseismic images for the paths 472 and 474, which have almost the same perpendicular baseline (B_{perp}) as the coseismic image pairs shown in Figure 3 (Table S1). Preseismic offset fields have little displacement (Figure S6), suggesting that the observed coseismic offsets exceed the potential error level significantly. The offset values in the basin are nearly zero; the root mean square (RMS) values are estimated to be ~0.1 m for both paths, but those in the mountains are not necessarily zero, particularly in high elevation areas; the RMS values are ~0.3 and ~0.4 m, for the paths 472 and 474, respectively. This may be because a correction of stereoscopic effect is insufficient because of the large amount of topographic relief. It is further noted that the displacement boundaries shown in Figure 3 are not seen in the preseismic data. This justifies our claim that the observed boundaries are not artifact but actual surface changes associated with the seismic event.

[16] The SAR images that include mountainous areas suffer strongly from foreshortening effects because of steep topography, which produces severe image distortion. Figure S7 shows the offset fields for the paths (a) 472 and (b) 474 calculated using the same preseismic data of Figure S6 but with no elevation-dependent correction.

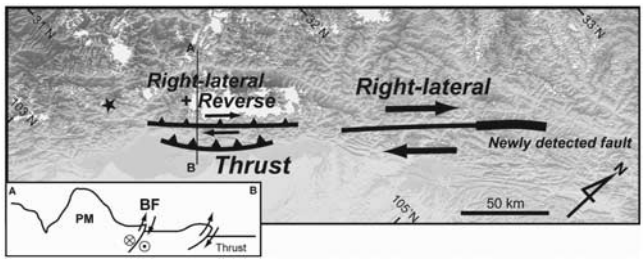

Figure 4. Schematic fault motions inferred from the offset fields. BF, Beichuan fault and PM, Pengguan massif.

Considerable offset errors, locally in excess of 3 m, correlating with the elevation are included. Although in principle the offset error caused by a stereoscopic effect should affect high topographic areas only, the poor global image coregistration resultantly gives more errors to the basin area as well. This result demonstrates that an elevation-dependent correction is indispensable for mountainous environments for extracting surface changes with high precision.

5. Summary

[17] We have successfully obtained ground displacements in the proximity of the Longmen Shan fault zone (LMSFZ) by an offset-tracking method, after applying an elevation-dependent correction. The outline of the inferred fault motions is illustrated in Figure 4 and the analysis results are summarized below.

[18] 1. A sharp displacement boundary, across which the ground movement is in the opposite direction, appears northeastward over a length of 200 km along the LMSFZ.

[19] 2. The main rupture has proceeded on the Beichuan fault (BF) among the several active faults composing the LMSFZ.

[20] 3. A new active fault is detected on the northeastward extension of the BF.

[21] 4. The rupture type is characterized by a right-lateral motion in the northeast on the BF, while an oblique slip consisting of right-lateral and reverse motions is suggested in the southwest.

[22] 5. Multiple ruptures including significant reverse slips occurred in the southeastern foot of the Pengguan massif.

[23] **Acknowledgments.** PALSAR level 1.0 data were provided from the Earthquake Working Group and PIXEL (PALSAR Interferometry Consortium to Study our Evolving Land surface) under a cooperative research contract with JAXA (Japan Aerospace Exploration Agency). The ownership of PALSAR data belongs to METI (Ministry of Economy, Trade and Industry) and JAXA. This study is supported from KAKENHI (19340123 and 20900002). We thank two anonymous reviewers and the editor (Fabio Florindo) for their helpful comments to improve our manuscript.

References

Avouac, J. P., F. Ayoub, S. Leprince, O. Konca, and D. V. Helmberger (2006), The 2005, M_w 7.6 Kashmir earthquake: Sub-pixel correlation of ASTER images and seismic waveforms analysis, *Earth Planet Sci. Lett.*, *249*, 516–528.

Burchfiel, B. C., L. H. Royden, R. D. van der Hilst, B. H. Hager, Z. Chen, R. W. King, C. Li, J. Lü, H. Yao, and E. Kirby (2008), A geological and geophysical context for the Wenchuan earthquake of 12 May 2008, Sichuan, People's Republic of China, *GSA Today*, *18*, 4–11, doi:10.1130/GSATG18A.1.

Bürgmann, R., P. A. Rosen, and E. J. Fielding (2000), Synthetic aperture radar interferometry to measure Earth's surface topography and its deformation, *Annu. Rev. Earth Planet. Sci.*, *28*, 169–209.

Densmore, A. L., M. A. Ellis, Y. Li, R. Zhou, G. S. Hancock, and N. Richardson (2007), Active tectonics of the Beichuan and Pengguan faults at the eastern margin of the Tibetan Plateau, *Tectonics*, *26*, TC4005, doi:10.1029/2006TC001987.

Farr, T. G., et al. (2007), The Shuttle Radar Topography Mission, *Rev. Geophys.*, *45*, RG2004, doi:10.1029/2005RG000183.

Gray, A. L., K. E. Mattar, and G. Sofko (2000), Influence of ionospheric electron density fluctuations on satellite radar interferometry, *Geophys. Res. Lett.*, *27*, 1451–1454.

Massonnet, D., and K. L. Feigl (1998), Radar interferometry and its application to changes in the Earth's surface, *Rev. Geophys.*, *36*, 441–500.

Michel, R., J.-P. Avouac, and J. Taboury (1999), Measuring ground displacements from SAR amplitude images: Application to the Landers earthquake, *Geophys. Res. Lett.*, *26*, 875–878.

National Earthquake Information Center (2008), Magnitude 7.9—Eastern Sichuan, China, U. S. Geol. Surv., Denver, Colo. (Available at http://earthquake.usgs.gov/eqcenter/eqinthenews/2008/us2008ryan)

Nishimura, N., and Y. Yagi (2008), Rupture process for May 12, 2008 Sichuan earthquake, Univ. of Tsukuba, Tsukuba, Japan. (Available at http://www.geol.tsukuba.ac.jp/~nisimura/20080512/)

Okada, Y. (1992), Internal deformation due to shear and tensile faults in a half-space, *Bull. Seismol. Soc. Am.*, *82*, 1018–1040.

Pathier, E., E. J. Fielding, T. J. Wright, R. Walker, B. E. Parsons, and S. Hensley (2006), Displacement field and slip distribution of the 2005 Kashmir earthquake from SAR imagery, *Geophys. Res. Lett.*, *33*, L20310, doi:10.1029/2006GL027193.

Strozzi, T., A. Luckman, T. Murray, U. Wegmuller, and C. L. Werner (2002), Glacier motion estimation using SAR offset-tracking procedures, *IEEE Trans. Geosci. Remote Sens.*, *40*, 2384–2391.

Tobita, M., M. Murakami, H. Nakagawa, H. Yarai, S. Fujiwara, and P. A. Rosen (2001), 3-D surface deformation of the 2000 Usu eruption measured by matching of SAR images, *Geophys. Res. Lett.*, *28*, 4291–4294.

Wegmüller, U., and C. L. Werner (1997), Gamma SAR processor and interferometry software, in *Proceedings of the 3rd ERS Symposium*, *Eur. Space Agency Spec. Publ.*, *ESA SP-414*, pp. 1686–1692.

Wegmüller, U., C. Werner, T. Strozzi, and A. Wiesmann (2006), Ionospheric electron concentration effects on SAR and INSAR, in *Proceeding of 2006 International Geoscience and Remote Sensing Symposium*, pp. 3731–3734, IEEE Press, New York.

M. Furuya and Y. Takada, Department of Natural History Sciences, Graduate School of Science, Hokkaido University, Kita 10 Nishi 8, Kita-ku, Sapporo 060-0810, Japan.

T. Kobayashi and M. Murakami, Institute of Seismology and Volcanology, Graduate School of Science, Hokkaido University, Kita 10 Nishi 8, Kita-ku, Sapporo 060-0810, Japan. (tkoba@uvo.sci.hokudai.ac.jp)